Proceedings of the ASME 2014 33rd International Conference on Ocean, Offshore and Arctic Engineering
OMAE2014
June 8-13, 2014, San Francisco, California, USA

OMAE2014-23715

SLAMMING LOADS CALCULATION FOR AN OIL TANKER

Chi-Chuan Chen **Chien-Hua Huang** **Kuan-Chen Chen** **Po-Wen Wang**

Research Department
CR Classification Society

ABSTRACT

The International Association of Classification Societies (IACS) Harmonised Common Structural Rules (CSR-H) have been released and will take effect on July 1, 2015. The local loads under extreme motion conditions, defined in the CSR-H, were investigated for an oil tanker by using computational fluid dynamics (CFD) software, STAR-CCM+, and included bow flare slamming pressure and bottom slamming pressure at the bottom of the bow or stern bottom. The extreme motion defined in the CSR-H was investigated using the potential code HydroSTAR. To benchmark the numerical results, resistance and seakeeping model tests were performed on the oil tanker. The two test results were simulated using the two software packages, respectively, and the numerical results were in good agreement with the test results. Finally, this study demonstrated that the slamming pressures defined by the CSR-H are safe and conservative with regard to the structural design.

1. INTRODUCTION

The extreme loads a ship carries over the duration of its life are regulated by the International Association of Classification Societies (IACS) Harmonised Common Structural Rules (CSR-H) [1] to comply with the International Maritime Organization (IMO) goal-based ship construction standards (GBS). The external slamming loads are stipulated in Chapter 4, Section 3 [1]. The slamming rules of the CSR-H are composed of 2-D and 3-D coefficients based on numerous investigations involving simulations or experiments.

The investigation of a simplified 2-D wedge entry problem was presented by von Karman [2]. Two-dimensional wedge simulations solved in potential theory have been developed and the water spray problem was remedied by Faltinsen [3].

Sebastiani et al. [4] investigated the effect of slamming loads on fast deep-V monohull vessels. The investigation demonstrated a zero forward speed 3-D correction to a 2-D representation of Wagner's formula, as well as a 3-D correction associated with a high forward speed calculated using model-scale and full-scale measurements. A stern slamming analysis involving 3-D computational fluid dynamics (CFD) simulations was investigated by Kim et al. [5]. In Kim et al.'s study, the impact velocity effect was investigated using CFD simulations. Slamming pressure was defined using Eq. (1), and was used to calculate k, where V_R is relative vertical velocity and k is the local pressure coefficient derived from the calculation.

$$p = \frac{1}{2}\rho k V_R^2 \tag{1}$$

Slamming occurs when the considered location is out of water and the relative velocity is above a certain threshold. A slamming pressure formula was deduced using probability analysis. Slamming pressures were then obtained from the CFD simulation of a 3-D stern hull, and various extreme velocities were evaluated by analyzing the loading conditions. k was calculated using the slamming pressures and extreme velocities. The results indicate that the variation of slamming pressure at a location can be attributed to the variation in the pressure coefficient more than it can be attributed to the variation in the extreme velocity. The American Bureau of Shipping (ABS) slamming pressure guide [6] was also calculated using 2-D formulas and 3-D corrections.

The slamming that occurs in a small region of bow areas was investigated by Azcueta [7]. The COMET which was the name of the viscous solver was employed to simulate the bow panel slamming pressure on a mega yacht. The rise time was less than 0.5 s. The results for the pressure peak were 170 to 270 KPa.

Deng et al. [8] focused on conducting numerical uncertainty estimations and suggested that incident waves with a fixed boat could be simulated accurately using approximately 100 time steps per period. However, a new time-step criterion is required for simulating strong pitch motion. The time discretization

error is higher than the spatial discretization error when less than 200 time steps per period are employed and when the ship's motion must be considered. Guo et al. [9] used the same settings [8] when they analyzed the ship's motion in waves, and they ensured that at least 70 cells per wavelength and 11 cells per wave height were present near the free surface. Their results regarding the motion in head waves were estimated accurately using both CFD and strip theory.

The time step and mesh requirements [9] were similar to those used in the CD-adapco [10]. The second-order method of analyzing time, which requires that the wave propagates less than half a cell per time step, was introduced. Using an order of 80 cells per wave length and 20 cells per wave height, and using the second-order scheme of time are essential for the accurate prediction of wave propagation.

Numerical simulations of slamming pressure were employed in this investigation using the commercial software STAR-CCM+. The particulars of an oil tanker are listed in Table 1. The grid independence was tested to ensure reliable results. The calm water resistance and the ship's motion in head waves with a small wave height were both simulated using STAR-CCM+.

The HydroSTAR software uses potential theory to solve the equations for describing the ship's motion. A comparison of the response amplitude operator (RAO) with regard to ship heave and pitch motion between the two software packages was performed to validate the results for the ship's motion.

Finally, extreme wave height was implemented in the slamming simulation. The pressure probes that were put onto the hull surface in advance were monitored through simulation time to observe when slamming occurred. The slamming pressure predicted using the Froude law was less than the pressure obtained from using the CSR-H.

Table 1. Oil tanker particulars

	Full-scale	Model-scale
Lpp(m)	174	4.35
Breadth(m)	32.2	0.805
Draught(m)	11	0.275
Cb	0.8186	0.8186
V	14.6(knots)	1.187(m/s)
Scale	40	

2. NUMERICAL METHODS AND GRID GENERATION

2.1 Physical models

The commercial code STAR-CCM+ was adopted to solve the Reynolds-Average Navier-Stokes Equation (RANSE) in the simulation. The software solves continuity and momentum equations and uses the pressure correction method, SIMPLE, to correct pressure and velocity. In the application of STAR-CCM+, the incompressible, implicit unsteady, and realizable k-epsilon two layer turbulence model was used in this study combined with a two-layer high y^+ wall treatment and the volume of fluid (VOF) method for two-phase flow. The simulation of an oil tanker's resistance in calm water employed the discretization of the first-order scheme in time and the second-order scheme in space. The second-order scheme in time was used in the simulation of an oil tanker's motion in head waves to improve accuracy.

STAR-CCM+ has an optional module with six DOFs (degrees of freedom) for conducting a simulation. The ship resistance in calm water was simulated by enabling two DOFs, translation in the draft direction (sinkage), and rotation in lateral direction (trim).

The simulations of the ship's motion in waves adopted the Stoke fifth-order wave, and the wave damping length was 0.5 L before the downstream boundary.

2.2 Mesh generation

Only half the computational domain was considered to reduce the computational capacity requirement because the simulation was symmetric. The coordinate origin was placed at the junction of the aft perpendicular and the baseline. The computational domain, as shown in Fig. 1, extended from -2 L to 2 L in the flow direction, from 0 to 1.5 L in the lateral direction, and from -1 L to 0.5 L in the vertical direction. The upstream boundary was located 1 L before the perpendicular and the downstream boundary was 2 L downstream from the aft perpendicular. Two lateral boundaries were located at 0 and 1.5 L. The bottom and top boundaries were located at -1 L and 0.5 L, respectively.

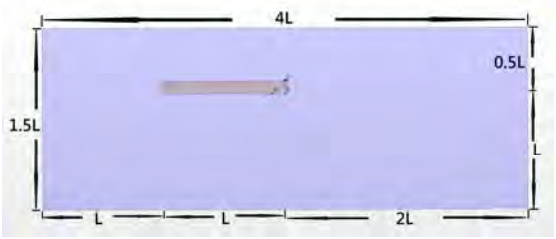

Figure 1. Side view of the computational domain (left side is the upstream boundary)

The boundary layer grid generated in STAR-CCM+ is called prism layers. Thickness, stretch factor (cell expansion ratio), and layers are the three parameters used by the software to generate the prism layer grid. In this simulation, the thickness was 0.02 m, the stretch factor was 1.3, and 15 layers were allocated to build the prism layer. For these setting, the y^+ values were maintained below 10 in the various speed calculations.

In addition to the prism layer, trimmer mesh was used to generate the computational domain and mesh topology, which was divided into three layers, as shown in Fig. 2. The grid size of the outer layer was twice as large as that of the inner layer. When the size of the inner layer was 2, then the intermediate layer was 4, and the outermost layer was 8. Grid refinements were employed in several regions such as the bow, stern, rudder, hull, wake, and free surface regions.

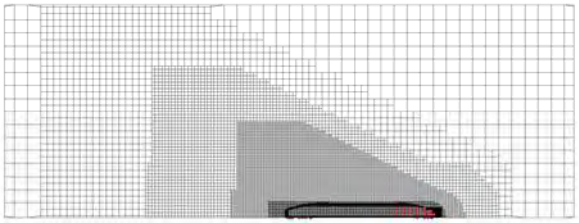

Figure 2. Top view of the computational domain

In the hull, wake, and free surface regions, the grid size of the refinement topology was three layers, as mentioned previously. The grid refinement of the free surface region was conducted in the x and y directions of the entire domain and in a section in the z direction. Figure 3 shows that the free surface refinement region of a section in the z direction was larger than that shown in Fig. 4. The grid size of the bow, stern, and rudder regions were the same or half the size of the neighboring cell, as shown in Figs. 3 and 4.

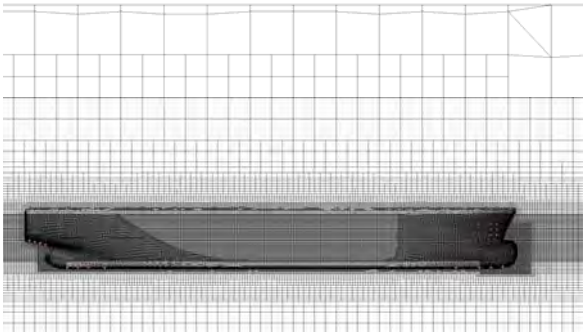

Figure 3. Side view near the hull

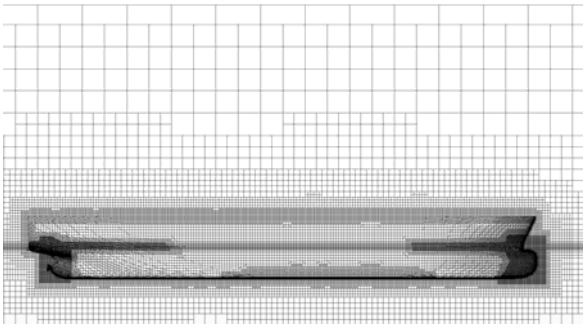

Figure 4. Side view near the hull

The grid setting shown in Fig. 3 was similar to that used in the previous motion test of Korea research institute of ship and ocean engineering (KRISO) container ship (KCS) with regard to incoming waves. The grid setting of Fig. 3 was first used in the calm water resistance calculation, and the friction results were determined to be dissatisfactory according to the formula developed by the International Tank Towing Conference (ITTC) (Eq. (2)). After changing the grid setting, as shown in Fig. 4, the friction results agreed with ITTC 1957 frictional formula, as shown in Fig. 7.

The grid setting shown in Fig. 5 incorporated the setting shown in Fig. 4 and included the free surface refinement. The top view in Figs. 5 and 2 show that the Fig. 5 grid setting used inside the free surface was a finer grid than that in Fig. 2, and that the Fig. 5 setting was used for calculating motion in waves solved with grid refinement.

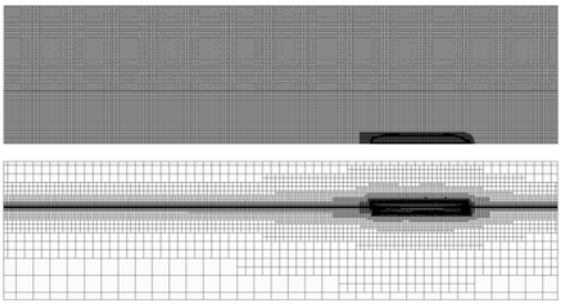

Figure 5. Top view (up) and side view (down) of the computational domain

In the settings shown in Fig. 5, which illustrates the free surface region, the cell points in the wave propagation direction were sufficient to perform wave calculations.

Before the simulation began, when the mesh generation was completed, the boundary conditions and initial conditions of the physical models could be given.

$$C_f = \frac{0.075}{(\log(Rn) - 2)^2} \tag{2}$$

2.2.1 Boundary and initial conditions

Upstream, the top, and bottom were treated as the inlet boundary conditions. The lateral boundary near the hull was a symmetrical plane, and the other lateral boundary was a slip wall boundary condition. Downstream was considered an outlet boundary condition.

The inlet initial condition was defined as the velocity and the hydrodynamic pressure of a flat VOF wave or VOF wave. The outlet pressure condition was defined as the hydrostatic pressure for the undisturbed water surface.

3. SIMULATION RESULTS

3.1 Calm water resistance

Calm water resistance was performed under a full-load condition and first order temporal discretization was used. The time step was 0.02 s and each time step had five inner iterations.

Three meshes based on altering only the base grid size by 0.035 m, 0.05 m, and 0.07 m were used. The other settings and y+ that were applied were the same in generating these three grids. The cell number of grids were 0.87 M, 1.4 M, and 2.1 M, respectively. These three grids were used to calculate the calm water resistance, and their friction forces were compared with the ITTC 1957 frictional formula (Eq. (2)).

As shown in Fig. 6, the 2.1M grid was adequate for resistance simulations. But the frictional force of a 1.4 M grid was near the ITTC frictional line. In this simulation, the 1.4 M grid was adopted to perform simulations at varying speeds.

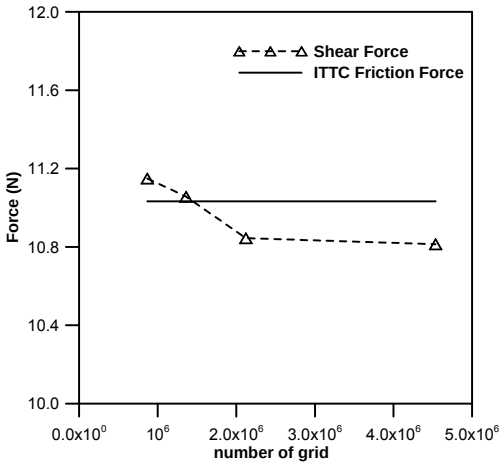

Figure 6. Results of friction force tests

The resistance, sinkage, and trim were included in the calm water resistance simulations and model tests using various speeds. Figure 7 shows that the frictional results at different speeds were in accordance with the ITTC formula, and that the difference was less than 3.6%.

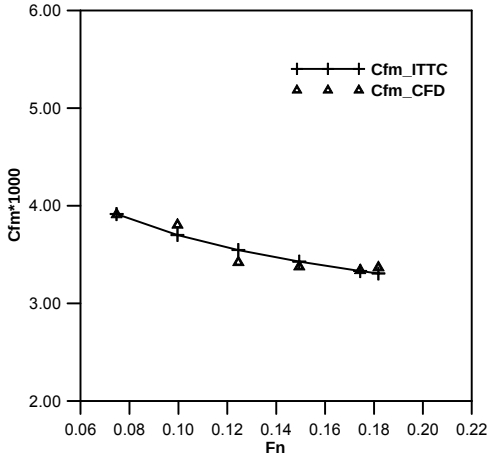

Figure 7. Friction force at various speeds

Based on the experimental data derived from the model tests, Fig. 8 shows that the CFD resistance was in accordance with that in the experimental data, besides two low speeds (Fn = 0.075 (6 kn) and 0.1 (8 kn)). The difference between these results was less than 4.2%.

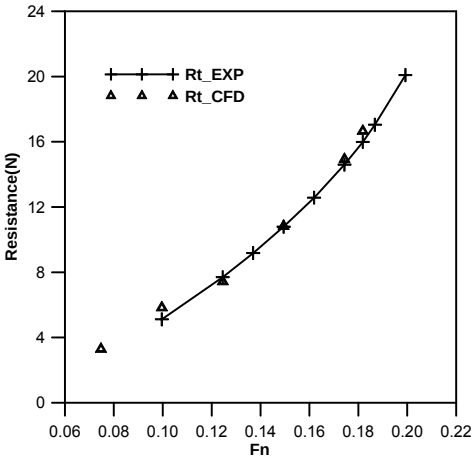

Figure 8. Total resistance force at various speeds

Figure 9 shows that model sinkage and trim exhibited the same trend and the same value. The total resistance coefficient (Ctm) is shown in Fig. 10. Besides two low speeds, the CFD results were similar to the experimental data. The residuary coefficient (Crm) was obtained from Eq. (3), as shown in Fig. 12.

$$C_{rm} = C_{tm} - C_{fm} \tag{3}$$

The Crm trend obtained from CFD was slightly higher than the experimental data. For a Fn value lower than 0.1, the Crm obtained using CFD was larger than that in the experimental data. For low speeds (Fn < 0.1), as shown in Fig. 7, STAR-CCM+ simulated the shear forces effectively, but insufficiently with regard to pressure forces, as shown in Fig. 11. The pressure force was not calculated precisely in these simulations.

The incorrect results obtained at low speeds could have been caused by the lack of software operations and grid generation techniques used, or the grid topology might not have been suitable for the low speed simulations.

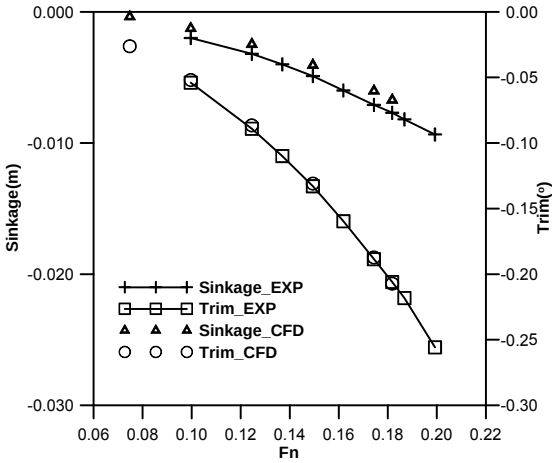

Figure 9. Sinkage and trim at various speeds

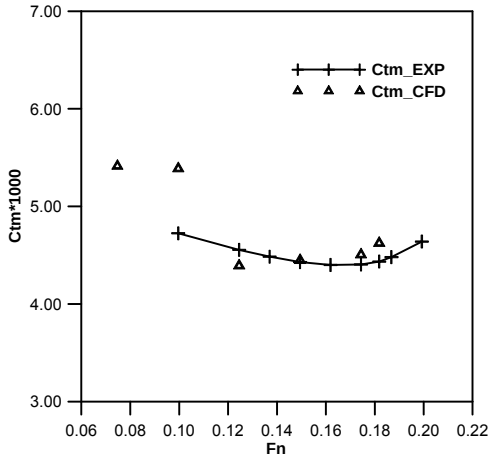

Figure 10. Ctm at various speeds

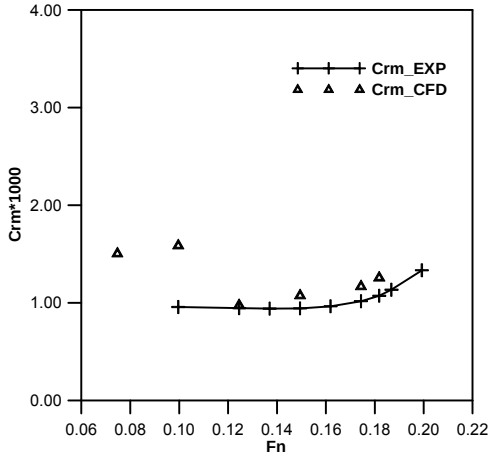

Figure 11. Crm at various speeds

3.2 Motion in waves

Motions that occur under wave conditions were calculated using the HydroSTAR and STAR-CCM+ software. Four scenarios were simulated in STAR-CCM+ and the wave length in all the simulations was larger than one ship length, and wave steepness was less than 1/91 (the wave height was maintained at a constant value of 0.05 m). Figs. 12 and 13 show the heave response amplitude operator (RAO), the pitch RAO results calculated using the two software packages, and the results obtained using HydroSTAR, which are marked with a "plus" symbol in the figures.

Employing the temporal discretization scheme, grid refinement, and time step could affect the results for the motion in waves. The major change in the results is shown in Fig. 12. r2 represents grid refinement, 1st represents the first-order scheme in time and 2nd represents the second-order scheme in time. The detailed comparison of the STAR-CCM+ software performance is introduced as follows.

Case 1: A calm water resistance grid was adopted to perform the motion in waves and first-order temporal discretization was used. The time step was 0.01 s. The results of this motion are marked with a diamond in Figs. 12 and 13. These results exhibit the same trend as and are less accurate than the HydroSTAR results.

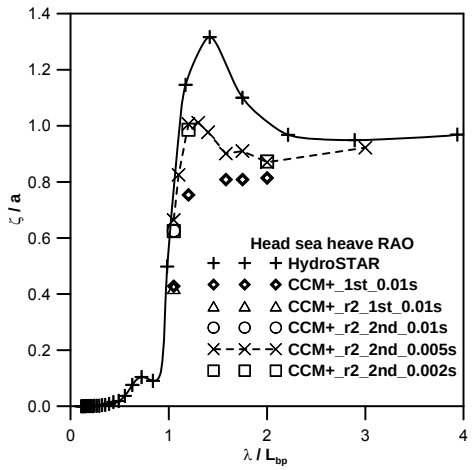

Figure 12. Results of the heave RAO

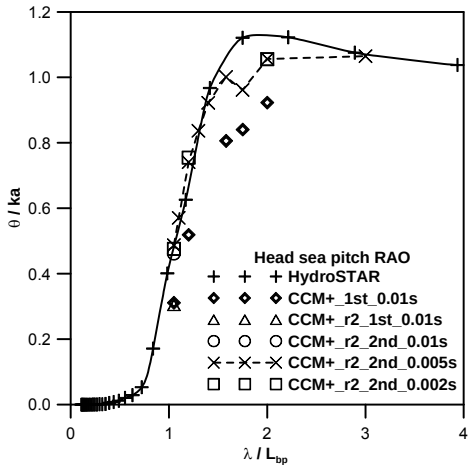

Figure 13. Results of the pitch RAO

Case 2: The point of the wave length was equal to 1.05 ship length. The setting of the mark of the triangle in the STAR-CCM+ simulation was added only to free surface refinement to achieve 80 cells per wave length, and this result was close to the case 1 result in the heave and pitch RAO. This indicates that grid refinement was unnecessary in this scenario. When the grid distribution complied with the minimal requirement of the wave simulations, the results of performing grid refinement produced a slight effect of the accuracy.

Case 3: By applying the settings used in Case 2, and changing the temporal discretization to the second-order scheme, the accuracy of the results, represented as a circle in Figs. 12 and 13, substantially improved in accuracy. The result of using the second-order scheme was more accurate with regard to time than that of the first-order scheme.

Case 4: Based on the settings used in Case 3, the time step was set to half of that applied in Case 3 (0.005 s) and the results are marked as crosses in Figs. 12 and 13. The RAO results maintained the same trend as that in the HydroSTAR results.

Case 5: Based on the settings used in Case 3, the time step was set to half of that applied in Case 4 (0.002 s) and the results are marked as square in Figs. 12 and 13. The RAO results maintained the same as case 4 results.

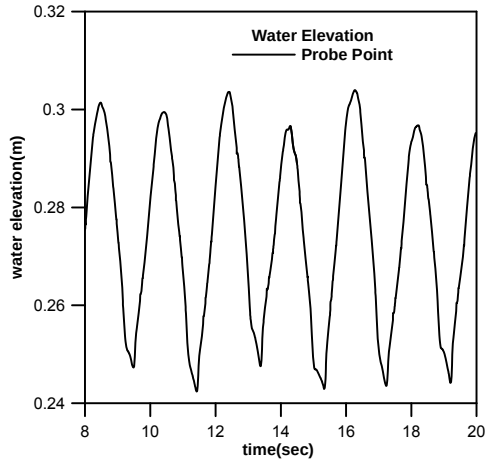

Figure 14. Water elevation analysis results

The point where the water elevation was analyzed was located on a free surface and the coordinate (x, y, z) values were at the fore perpendicular, away from the ship (y = 6) and on the free surface, respectively. The model wave height was 0.05 m and the water elevation was between 0.25 m and 0.3 m. The water elevation analysis was drawn as a time sequence, as shown in Fig. 14, and the water elevation was nearly 0.05 m. The pressure probe acquired data at several predetermined locations (Table 2 and Fig. 15). Figure 16 shows that the probe pressure at these three points was caused by static water pressure at the 0.05-m wave height. No slamming occurred at these points. Bottom slamming at a small wave height was not considered.

4. SLAMMING PRESSURE COMPARED WITH THE CSR-H

The CSR-H rules for regulating extreme loads were designed based on a ship's life (corresponding to a probability level of 10^{-8}). Regarding the wave condition, according to IACS Recommendations 34, wave scatter diagram for the North Atlantic, and ABS slamming guides [6], an extreme wave height of 14.8 m and a zero-crossing period of 10.5 s was employed in the slamming simulation. A regular wave was used in the simulations and the wave steepness was 1/12.4.

In this extreme wave height simulation, the simulation was set up on a model scale, and the forward velocity was 0.81 m/s (10 kn for full scale ship). The first-order temporal scheme was adopted to maintain stability, because the solution in which the second-order scheme was used diverged and caused the simulation process to stop.

Table 2. Analysis point locations and predicted pressure

Bow flare point	Location(x/L, z/D), y = hull surface	CSR-H (kPa)	Predicted pressure (kPa)
35	(0.95, 1.091)	204	143
36	(0.95, 1.273)	236	123
37	(0.95, 1.455)	261	91
38	(0.975, 1.091)	233	187
39	(0.975, 1.273)	263	180
40	(0.975, 1.455)	286	151
41	(0.9875, 1.091)	207	197
42	(0.9875, 1.273)	247	208
43	(0.9875, 1.455)	269	173

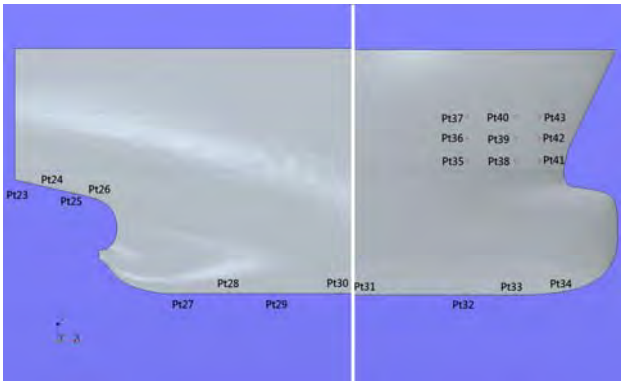

Figure 15. Analysis point locations

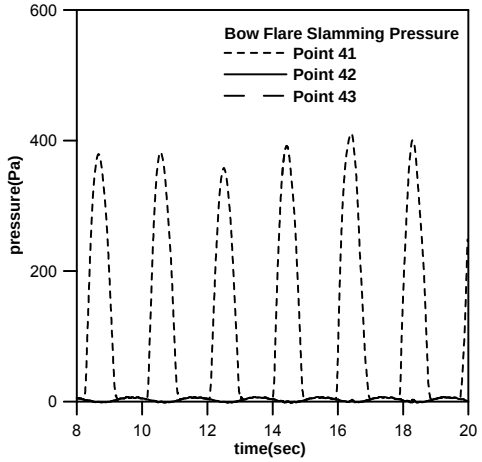

Figure 16. Pressure at bow flare points

This slamming simulation was constructed before simulating the ship's motion when a small wave height was used, because several simulations of the KCS of the ship's motion with regard to waves had been previously completed.

The grid generated based on the settings used in Case 1 were implemented, but the free surface layer thickness in the z direction (Fig. 3) was designed to be larger than that in Case 1, as shown in Fig. 4.

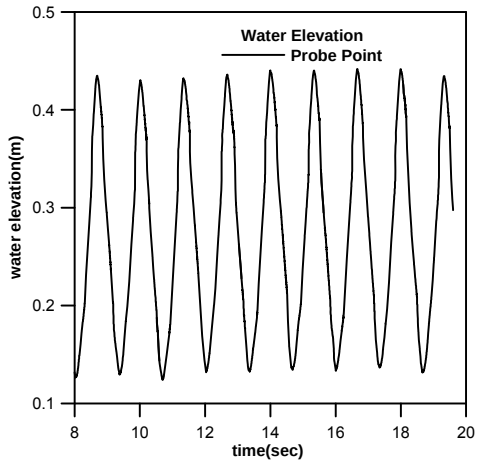

Figure 17. Water elevation analysis results

To achieve a short duration for the slamming pressure phenomenon, the time step used in this simulation was set to 0.002 s and one wave period was divided into 850 time steps.

Figure 17 shows the water elevation and that the wave height did not decay as the time increased.

Pressure probes were used to observe pressure variations at nine points in the bow flare areas. Three points were selected from the longitudinal and draught directions, as listed in Table 2.

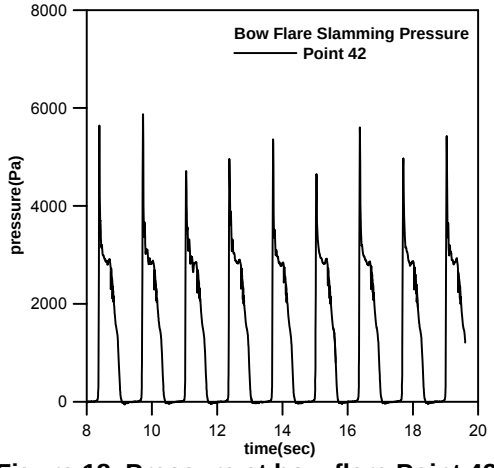

Figure 18. Pressure at bow flare Point 42

Figure 18 shows the slamming pressure at Point 42 with time. The peak value oscillates at approximately 5300 Pa and the second small peak pressure appears repeatedly.

Figure 19 shows only one period of slamming pressure. The duration of this period was less than 1 s and the time taken for the pressure to rise to peak pressure was approximately 0.1 s or less. To obtain this peak value, the simulation time step was at less than 0.1 s. The time step effect for the peak pressure during the pressure rise time are required to resolve and this study does not contain time step effect for slamming.

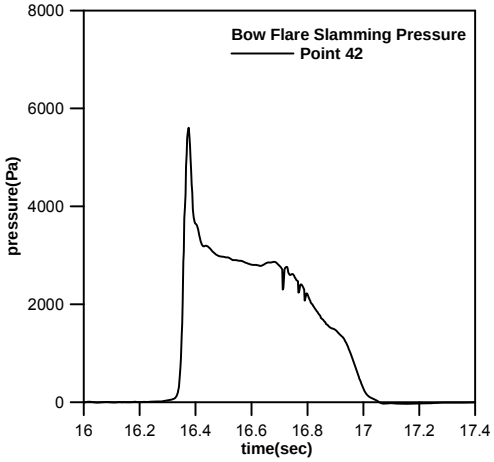

Figure 19. Pressure at bow flare Point 42 over one period

The mean pressure (2121 Pa) for the entire period was smaller than the peak pressure (5204 Pa). The peak pressure was used to predict the full-scale ship slamming pressure, which is listed in Table 2.

The bow impact pressure stipulated by the CSR-H was obtained using Eq. (4)–(6) and the results are listed in Table 2. Equations (4) involves the effects of longitudinal and vertical locations, impact velocity, and local impact geometry, which is the same meaning as the equation used in [6].

$$P_{FB} = 1.025 \times f_{FB} \times c_{FB} \times V_{im}^2 \times \sin\gamma_{wl} \quad (4)$$

$$V_{im} = 0.514 \times V_{ref} \times \sin\alpha_{wl} + \sqrt{L} \quad (5)$$

$$V_{ref} = 0.75V \quad (6)$$

Table 2 shows that the slamming pressure, when applying the CSR-H, was larger than the pressure predicted by the STAR-CCM+ simulation. The slamming pressures stipulated by the CSR-H, are safe and conservative with regard to the structural design.

Table 3. Probe points at bottom locations

Bottom point	Location(x/L, z), y=0
27	(0.069, 0)
29	(0.115, 0)
30	(0.15, 0)
31	(0.9, 0)
32	(0.95, 0)
33	(0.975, 0)
34	(1.0, 0)

Several pressure probes were located on the bottom surface of the stern and bow, as shown in Table 3 and Fig. 15. The bottom pressure results are shown in Figs. 20–22. Because of the draught (0.275 m) and wave height (0.37 m) used in this simulation, the hydrostatic pressure caused by the underwater depth (0.46 m) was approximately 4500 Pa. Figure 20 shows that the bottom pressure at the stern oscillated between 2000 Pa and 3500 Pa. The pressure at these points was lower than the hydrostatic pressure. Slamming at the bottom of the stern rarely occurs under full-loading conditions.

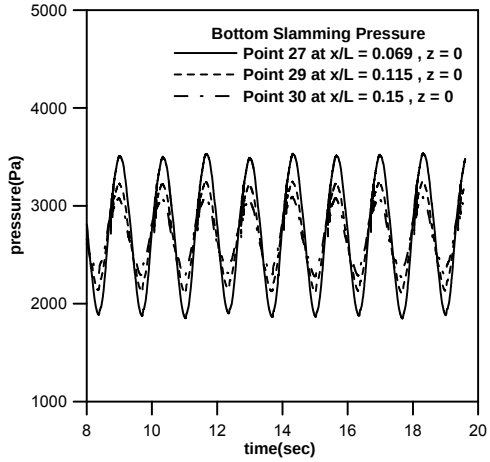

Figure 20. Pressure at the stern bottom

The pressures at the bottom of the stern near after-perpendicular(AP) are shown in Fig. 21, and the pressure variations were between 0 Pa and 1500 Pa. The pressure decreased to 0 Pa, indicating that the probe point could have been above the surface of the water and that slamming occurred at a low pressure.

The pressures at the bottom of the bow are shown in Fig. 22, and the pressure variations were between 0 Pa and 5600 Pa. The peak pressure at the bottom of the bow was larger than the peak pressure at the bottom of the stern, indicating that slamming occurred. When the pressure decreased to 0 Pa, the probe point was possibly above the water surface. When the pressure increased to 5600 Pa, the probe point may have been immersed in the water again. Thus, slamming was confirmed to occur during this period. The pressure observed in the simulation under full-loading conditions was not compared with that defined in the CSR-H, because the bottom slamming formula stipulated by the CSR-H considers a ballast condition.

The rigid body angular velocity and relative velocity can be calculated in the STAR-CCM+. The vertical velocity for the hull could be derived from the angular velocity multiplied by the distance from LCB to considered points. The vertical velocity was considered with hull motion and listed in Table 4. The angular velocity obtained from STAR-CCM+ and the vertical velocity of two points predicted by Froude law were less than CSR-H values. The vertical velocity was less than the CSR-H impact velocity was reasonable.

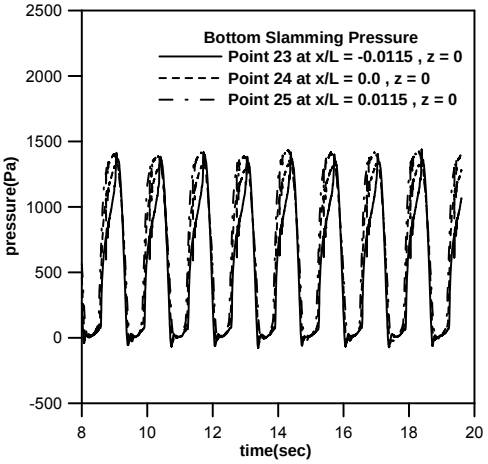

Figure 21. Pressure at the stern bottom near AP

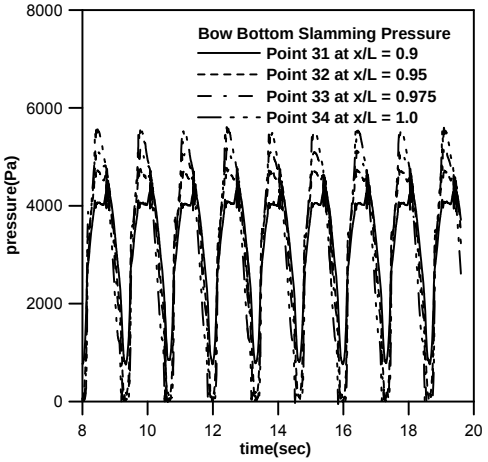

Figure 22. Pressure at the bow bottom points

Table 4 Impact velocity at considered point

		point 39	point 42
model scale	distance to LCB	1.943	1.997
	vertical velocity (m/s)	0.894	0.919
	Maximal angular velocity (rad/s)	-0.4215	-0.4215
	vertical velocity (m/s)	-0.819	-0.842
full scale	vertical velocity (m/s)	-5.180	-5.324
	Vim (knots)_ CSR-H	16.139	16.139
	Vim (m/s)_ CSR-H	8.302	8.302

The second-order scheme in time was more accurate and less stable than the first-order scheme in time [10]. Mesh and time step conditions must be in accordance with those used in the second-order scheme in time to achieve stability and solve the equations accurately from these cases experience of using STAR-CCM+. Based on simulated tests using the second-order scheme in time demonstrated in [10], each wave length had at least 80 cells and 20 cells per wave height, and one period

comprised 100 time steps, the wave to be solved accurately using the second-order scheme in time.

In all of the scenarios, one wave period comprised at least 170 time steps (or 340) and the cell number per wave length had sufficient resolution (at least 80) under an even keel condition, but reduced resolution when the computational domain rotated with a pitch motion. The technique of rotating the computational domain with the ship's motion requires a large number of cells aligned with the free surface to improve the accuracy of simulating the ship's motion in the wave.

In certain scenarios, using the first-order scheme in time was a compromise to obtain results, and these results should be considered carefully.

5. CONCLUSION

In this study, several goals were achieved and STAR-CCM+ simulations were completed successfully.

1. The calm water resistance simulations were performed successfully.

2. Simulations of motion at a small wave height were performed to compare the results with those obtained using the HydroSTAR software, and the results exhibited the same trend.

3. A simulation of motion in waves with an extreme wave height was conducted. The predicted pressure was compared with the pressure obtained from the CSR-H. The predicted pressures were smaller than the pressure specified in the CSR-H, indicating that the CSR-H pressures are safe and conservative with regard to structural design.

The simulation must be analyzed precisely, or a comparison between the simulation data and real data should be conducted. The results of the extreme simulations require additional validation, such as the process of motion in waves with small wave heights.

To obtain reliable results, the techniques used in the second-order scheme in time will be adapted to perform adequate simulations in the future. Full-scale simulations will be used to validate the accuracy of the prediction made using the Froude law.

NOMENCLATURE

L : Ship length between perpendicular in m
Lpp : The same as L
Cb : Block coefficient
p : Pressure or slamming pressure
ρ : Density of water
k : Local pressure coefficient derived from the calculation
V_R : Relative vertical velocity
λ : Wave length in m
Rn : Reynolds number
Fn : Froude number
V : Ahead maximum service speed in kn
Ct : Total resistance coefficient
Cf : Friction resistance coefficient
Cr : Residuary resistance coefficient
f_{FB} : Longitudinal bow flare impact pressure distribution factor
C_{FB} : Draught position coefficient
α_{wl} : Local waterline angle, in deg, at the considered position, but not less than 35°
β_{pl} : Local body plan angle, in deg, at the considered position from the horizontal to the tangent line, but not less than 35°
γ_{wl} : Local bow impact angle, in deg, at the considered position, but not less than 35°, measured in drawing or obtained using the following equation:

$$\gamma_{wl} = \tan^{-1}\left(\frac{\tan\beta_{pl}}{\cos\alpha_{wl}}\right)$$

REFERENCES

[1] CSR-H, "Common Structural Rules for Bulk Carriers and Oil Tankers," 2013, IACS.

[2] Karman, von, "The impact of seaplane floats during landing," NACA Technical Report 321,1929.

[3] Faltinsen, O. M., " Water entry of a wedge with finite deadrise angle," Journal of ship research, 46, 1, pp. 39–51, March 2002.

[4] SEBASTIANI, L., Valdenazzi, F., Grossi, L., Kapsenberg, G. K., " A theoretical / experimental investigation of the slamming pressures on fast monohull vessels," FAST2001.

[5] Kunho Kim, Yung S. Shin, "A stern slamming analysis using three-dimensional CFD simulation," OMAE 2008-57805, (ABS technical papers).

[6] Guide for slamming loads and strength assessment for vessels, ABS.
https://www.eagle.org/eagleExternalPortalWEB/ShowProperty/BEA%20Repository/Rules&Guides/Current/177_Slamming/Guide

[7] Azcueta R., "Slamming pressures on a mega yacht by means of RANSE simulations," internal report, 2004, Cape Hom Engineering, Spain. http://www.cape-horn-eng.com/archives/publications/Azcueta_str2004.pdf

[8] Deng, G.B., Queutey, P., Visonneau, M., " RANS prediction of the KVLCC2 tanker in head waves," 9th international conference on hydrodynamics, 2010, Shanghai, China.

[9] Guo, B.J., Steen, S., Deng, G.B., " Seakeeping prediction of KVLCC2 in head waves with RANS," Applied Ocean Research, 35, pp.56-67, 2012.

[10] Milovan Perić, "Wave Impact, Body Motion and Overset Grids in STAR-CCM+", STAR South East Asian Conference, 2012. http://www.cd-adapco.com/sites/default/files/Presentation/WavesBodyOverset_MP.pdf